

Hsa_circ_0021727 (circ-CD44) promotes ESCC progression by targeting miR-23b-5p to activate the TAB1/NFκB pathway

Fan Meng

The First Affiliated Hospital of Gannan Medical University

Xiaokang Zhang

The First Affiliated Hospital of Gannan Medical University

Yanting Wang

The First Affiliated Hospital of Gannan Medical University

Jie Lin

The First Affiliated Hospital of Gannan Medical University

Yulin Tang

The First Affiliated Hospital of Gannan Medical University

Guisheng Zhang

The First Affiliated Hospital of Gannan Medical University

Binqiang Qiu

The First Affiliated Hospital of Gannan Medical University

Xingdu Zeng

The First Affiliated Hospital of Gannan Medical University

Weiyu Liu

The First Affiliated Hospital of Gannan Medical University

Xin He (✉ hexin@gmu.edu.cn)

The First Affiliated Hospital of Gannan Medical University

Research Article

Keywords: hsa_circ_0021727, ESCC, miR-23b-5p, TAB1, progression

Posted Date: June 24th, 2022

DOI: <https://doi.org/10.21203/rs.3.rs-1760281/v1>

License:   This work is licensed under a Creative Commons Attribution 4.0 International License.

[Read Full License](#)

Abstract

Background: The morbidity and mortality of esophageal squamous cell carcinoma (ESCC) remain high globally. Circular RNAs (circRNAs) play an important role in tumor progression. We discovered a novel aberrantly expressed circRNA (hsa_circ_0021727) in ESCC patients. However, the mechanism of hsa_circ_0021727 in tumors is still not elucidated. The purpose of this article is to investigate the biological role of hsa_circ_0021727 and its role in ESCC progression.

Methods: Microarray analysis was used to screen differentially expressed novel circRNAs. qRT-PCR, RNA-ISH and FISH were used to analyze the expression and localization of hsa_circ_0021727. MTT, colony formation, EdU, transwell assay, three-dimensional (3D) spheroid invasion assays and wound healing assays were used to describe biological effects on ESCC cells. Xenograft experiment and tail vein injection experiment were used to analyze tumor growth and metastasis in vivo. RNA-sequencing was used to identify hsa_circ_0021727 downstream targets. Western blot was used to detect the downstream protein expression of hsa_circ_0021727. RNA pulldown and dual luciferase experiments were used to evaluate the interaction of hsa_circ_0021727, miR-23b-5p and TAB1.

Results: We screened a novel circRNA (hsa_circ_0021727) whose expression was upregulated in ESCC patients. ESCC patients with high expression of hsa_circ_0021727 had shorter survival time. Hsa_circ_0021727 promoted the proliferation, invasion and migration of ESCC cells. However, miR-23b-5p inhibited this ability of hsa_circ_0021727. MiR-23b-5p acts by targeting TAB1. In conclusion, hsa_circ_0021727 promoted ESCC progression by upregulating the expression of TAK1-binding protein 1 (TAB1) via "sponge adsorption" of miR-23b-5p. In addition, in vivo experiments also confirmed that hsa_circ_0021727 can promote the proliferation, invasion and migration of ESCC cells.

Conclusions: Hsa_circ_0021727 (circ_CD44) promotes ESCC progression by targeting miR-23b-5p to activate the TAB1/NF κ B pathway. These findings may provide potential targets for the treatment of ESCC.

Background

There were 604,100 new cases of esophageal cancer worldwide in 2020, accounting for 3.1% of all cancer cases and ranking the eighth, and the number of deaths reached 544,076, accounting for 5.5%, ranking the sixth [1, 2]. ESCC and esophageal adenocarcinoma are the two main pathological subtypes of esophageal cancer, and ESCC is the predominant in China [3]. At present, the vast majority of ESCC patients are in the middle and late stages when they are diagnosed, losing the chance of cure, and the 5-year survival rate is less than 20% [4, 5]. The etiology of ESCC is still unclear. Previous studies have shown that chronic esophageal injury, esophageal inflammation, and changes in gene expression caused by high-temperature diet or alcohol consumption may be associated with ESCC [6, 7, 8]. In recent years, with the in-depth research on the pathogenesis of esophageal squamous cell carcinoma, finding more reliable targets has become an extremely urgent task.

After the completion of the Human Genome Project, it was found that only 2% of the genes have functions to stably transcribe and translate proteins, while the vast majority are non-coding RNAs (ncRNAs)[9, 10]. CircRNA is a special kind of ncRNA molecule, which is involved in the pathogenesis of various diseases. Different from traditional linear RNAs, circRNA molecules have a closed ring structure, which is not affected by RNA exonuclease, and the expression is more stable and not easy to be degraded. CircRNA play an important role in malignant tumors, cardiovascular and cerebrovascular diseases, diabetes and other diseases[11, 12, 13]. A large number of circRNAs are widely involved in various stages of cancer occurrence and development. ESCC was also found to be highly correlated with the expression of circRNAs. For instance, nuclear genome-derived circular RNA circPUM1 localized in mitochondria and regulates oxidative phosphorylation in esophageal squamous cell carcinoma[14]. CircRNA-DOPEY2 was found to enhance chemosensitivity of esophageal cancer cells by inhibiting CPEB4-mediated translation of Mcl-1[15]. Circular RNA hsa_circ_0000277 sequesters miR-4766-5p to upregulate LAMA1 and promote esophageal carcinoma progression[16]. CircGSK3 β is thought to promote the metastasis of esophageal squamous cell carcinoma by enhancing β -catenin signaling[17]. Our understanding of circRNAs is still at a very superficial stage. Therefore, the molecular mechanism of circRNAs in ESCC deserves our in-depth study.

A newly discovered circRNA, hsa_circ_0021727 is annotated as a ncRNA located on chr11, and its function has not been studied. Among the molecular mechanisms of circRNAs that have been reported, the most common one is to competitively bind to certain microRNAs (miRNAs), acting as an "adsorption sponge" for miRNAs, preventing miRNAs from interacting with mRNAs in the 3' untranslated region, thereby indirectly regulating the downstream targets of miRNAs gene expression[18, 19].

MiRNAs are a class of non-coding single-stranded RNA molecules of about 22 nucleotides in length encoded by endogenous genes, which are involved in post-transcriptional gene expression regulation in animals and plants[20]. These small RNAs have a wide range of roles in the regulation of eukaryotic gene expression. Their mechanisms include severing mRNA molecules of target genes and inhibiting translation of target genes[21, 22]. For example, MiR-153-3p is thought to reduce extracellular matrix accumulation in high glucose-stimulated human mesangial cells by targeting PAQR3 in diabetic nephropathy[23]. Exosomal microRNAs induce tumor-associated macrophages via PPAR γ during tumor progression in SHH medulloblastoma[24]. Downregulation of ZC3H13 by miR-362-3p/miR-425-5p is associated with a poor prognosis and adverse outcomes in hepatocellular carcinoma[25]. In this study, miR-23b-5p, as a downstream molecule of hsa_circ_0021727, also played an important role in the progression of ESCC.

In order to explore the role of circRNAs in the occurrence and development of ESCC, we detected the expression of circRNAs in ESCC patient tissues, screened circRNAs that may be targets for early diagnosis and treatment of ESCC, and clarified their possible molecular mechanisms.

Materials And Methods

Clinical tissue specimens

We collected 8 cancer tissue samples of ESCC. All samples were from the First Affiliated Hospital of Gannan Medical College, from January to December in 2019. After the surgical operation, tissue specimens were frozen in liquid nitrogen immediately. None of these patients had received radiation or chemotherapy. All patients were well informed, the processes were approved by Ethics Committee of The First Affiliated Hospital of Gannan Medical University, and written informed consent was obtained from each patient.

Two tissue microarrays were used to evaluate the expression of hsa_circ_0021727 by ISH. The tissue microarrays were purchased from Shanghai Outdo Biotech Co., Ltd. (Shanghai, China) and contained approximately 170 pairs of ESCC samples and 100 pairs of their para-carcinoma tissues. Patients were selected based on a clear pathological diagnosis of early stage (Stages IA-IIIa) ESCC. All patients' follow-up records were collected from January 2006 to July 2015.

CircRNA microarray

In order to screen out circRNAs that can be used as targets, we performed circRNA microarray hybridization and data analysis on the three pairs of tissue samples collected. Total RNA was digested with RNase R (Epicentre, USA) to remove linear RNAs and enrich circRNAs. Then, the enriched circRNAs were amplified and transcribed to fluorescent cRNA utilizing a random priming method (Arraystar Super RNA Labeling Kit; Arraystar; USA). The labeled cRNAs were hybridized to an Arraystar Human circRNA Array (8x15K, Arraystar). After washing the slides, the arrays were scanned with an Agilent G2505C scanner. Agilent Feature Extraction software (version 11.0.1.1) was used to analyze the acquired array images.

CircRNA in situ hybridization (RNA-ISH)

All experimental steps will be performed according to the standard procedures of ISH[26]. Tissue microarrays were deparaffinized, rehydrated through an ethanol gradient, and then treated with 20 µg/mL proteinase K (Roche Diagnostics, Indianapolis, IN). Then, it was fixed with formaldehyde (Thermo Scientific, Rockford, IL), rinsed twice with 0.13 M 1-methylimidazole, and finally fixed again with 1-ethyl-3-(3-dimethylaminopropyl) carbodiimide (EDC, Thermo Scientific). After blocking endogenous peroxidase in H₂O₂, prehybridization buffer was performed, and slides were finally hybridized with 200 nM digoxigenin (DIG) LNA modifications.

Two pathologists blinded to clinical data scored tissue microarray staining independently using the following criteria. Two senior pathologists were blinded to patients' outcome and assigned to evaluate the immunoreactivity independently. Intensity of immunostaining was scored as 0 (no immunostaining), 1 (weak immunostaining), 2 (moderate immunostaining), and 3 (strong immunostaining). The percentage of immunoreactive cells scoring was documented as 0 (none), 1 (< 20%), 2 (20–50%), 3 (51–75%), and 4 (> 75%). Cutoff values for low and high expression groups were determined by using the degree × intensity

staining rank. Low expression was defined as a final score < 6 and high expression was defined as a final score ≥ 6 .

Cell culture

Human ESCC cell lines (TE-1 and KYSE-510) were purchased from American Type Culture Collection (USA). All cells were prepared in 10% fetal bovine serum(FBS; Gibco, USA) in RPMI 1640 medium (Gibco, USA). Culture dishes containing cells were incubated at 37°C in humidified air with 5% CO₂.

Total RNA extraction and quantitative real-time PCR (qRT-PCR)

Total RNA was extracted from frozen tissues and cells using RNAiso Plus (Takara, Japan) according to the manufacturer's instructions. RNA level was measured by qPCR with the SsoFast EvaGreen Supermix (Bio-Rad Laboratories, Hercules, CA), and the glyceraldehyde-3-phosphate dehydrogenase (GAPDH) was used as an internal reference.cDNA was synthesized using PrimeScript RT Master Mix(Takara, China). qPCR was performed with TB Green Premix Ex Taq II (Takara, China) with the following thermal cycling program: 95°C for 30 s and 40 cycles at 95°C for 5 s, 60°C for 30 s, and a dissociation step.All primer sequences are recorded in Table S2.

Cell transfection

CircRNA overexpression and short hairpin RNA (shRNA) lentiviral vectors, miRNA lentiviral vectors, and matching negative control vectors were designed and synthesized by Synbio Technologies (Suzhou, China).Short interfering RNA (siRNA) sequences were directly synthesized (GenePharma, Shanghai, China).Use Lipofectamine 3000 (Invitrogen, Carlsbad, CA) to transfect cells with designated lentiviral vectors according to the manufacturer's instructions. All shRNA sequences were listed in Table S3A.

RNA (shRNA) lentiviral vectors, miRNA lentiviral vectors, and matching negative control vectors were designed and synthesized by Synbio Technologies (Suzhou, China).Short interfering RNA (siRNA) sequences were directly synthesized (GenePharma, Shanghai, China).Use Lipofectamine 3000 (Invitrogen, Carlsbad, CA) to transfect cells with designated lentiviral vectors according to the manufacturer's instructions. All shRNA sequences were listed in Table S3A.

Fluorescence in situ hybridization (FISH)

We purchased FISH probes designed by RiboBio (Guangzhou, China).Cy3-labelled probes and FAM-labelled probes were used as mark for hsa_circ_0021727 and miRNA-23b-5p(Table S2B).Nuclei were stained with 4',6-dimethyl-2-phenylindole (DAPI).The assay was performed according to the instructions of the FISH kit (Gene Pharma, China).Stained pictures were observed and acquired by confocal microscopy (Leica, Germany).

Cell proliferation, colony formation assays and 5-Ethynyl-2'-deoxyuridine (EdU) incorporation assay

[4,5-Dimethylthiazol-2-yl]-2,5-diphenyltetrazolium bromide (MTT) determination was used for the assessment of cell proliferation. The transfected cells were seeded in a 96-well plate, then 20 μ l of 5mg/mL MTT solution (MTT Cell Proliferation and Cytotoxicity Assay Kit, BOSTER, China) was added to incubate for 4 hours, and finally 100 μ L of dimethyl sulfoxide was added. The microplate reader measures the optical density at 490 nm.

Colony formation assays, divide the transfected cells into 6-well plates (1000 cells/well). After 2 weeks in culture, cells were fixed with 75% ethanol and finally stained with 0.2% crystal violet. The colony formation rate was determined by counting the number of stained colonies.

ethynyl-2'-deoxyuridine (EdU) immunofluorescence assay was performed with Cell-Light EdU DNA Cell Proliferation Kit (RiboBio, Guangzhou, China) according to the manufacturer's instructions. Treated esophageal squamous cell carcinoma cells were incubated with EDU for 3 hours. After fixation and permeabilization, anti-EdU reagents and DAPI were used for cell staining. Fluorescence microscopy was used to observe and obtain pictures.

Cell invasion, migration, wound healing assay

For the invasion assay, medium was added to the chamber after precoating the chamber membrane with 100 μ L of Matrigel (BD Bioscience, San Jose, CA, USA). Then added 100 μ L of serum-free medium to the transfected cells for use. Cells were added to the upper chamber, complete medium was added to the lower chamber, and sequentially incubated at 37°C in 5% CO₂ for 24 h. Finally, fixed with 4% paraformaldehyde solution and stained with 0.1% crystal violet solution. We obtained pictures using an inverted fluorescence microscope using Olin and counted these cells.

Three-dimensional (3D) spheroid invasion assays were used to detect the invasive ability of tumor cells. Transfected cells were seeded in ultra-low attachment (ULA) round-bottom 96-well plates for 4 days, allowing them to form tumor spheroids. Then, added 100 μ l of basement membrane matrix (BMM, Corning) to each well for centrifugation and incubated at 37°C for one hour to solidify. Finally, 100 μ l of medium containing 10% FBS was added to each well and incubated at 37°C in 5% CO₂. We obtained images with an inverted microscope.

For wound healing assay, transfected cells were added to a six-well plate culture in serum-free medium, followed by scraping with a pipette tip to form a cell monolayer. Representative images of cell migration were captured at 0 h and 24 h after linear wound formation. We assessed wound healing and obtained pictures by microscopy.

Western blot analysis

We added RIPA buffer to the transfected cells, then took the supernatant and added protease inhibitor (1%; ComWin Biotech, Beijing, China). Protein concentration was checked by BCA Kit (Biyotime Biotechnology). Equal amounts of protein were separated by SDS-PAGE (10% or 8%) and transferred to 0.45 μ m PVDF membranes (Roche, Indianapolis, IN). After blocking with 5% nonfat milk for 1 hour, PVDF

membranes were incubated with primary antibody overnight at 4°C. Membranes were washed a minimum of 3 times in TBST for 10 min each, followed by one hour incubation with goat anti-rabbit or goat anti-mouse secondary antibodies. Finally, the membrane was washed 3 times with TBST again. Protein bands were detected with

SuperSignal West Femto Agent (Millipore) and visualized with the Chemical Mp Imaging System (Bio-Rad). The antibodies are listed in Table S4.

RNA pull-down assay

A hsa_circ_0021727 biotin-conjugated probe and oligo probe (Table S3B) were designed by RiboBio (Guangzhou, China). The treated cells were added to the lysate and incubated with streptavidin magnetic beads (Life Technologies, USA) for 2 hours. The cell lysates were incubated with probe-coated beads at 4°C overnight. The beads were washed five times repeatedly, then the bound miRNAs in the pull-down material were extracted using Trizol reagent and analyzed by qRT-PCR analysis.

Luciferase reporter assay

After designing and synthesizing wild-type and mutant vectors, ESCC cells were co-transfected with other lentiviral vectors. Cell lysates were added after 48 hours, and luciferase activity was analyzed by a dual-luciferase reporter gene assay system (Promega, USA).

RNA-seq assay

Total RNA of ESCC cells was extracted in accordance with the manual of TRIzol® reagent (Invitrogen, Shanghai, China). The libraries were then constructed using TruSeq Stranded Total RNA with Ribo-Zero Gold according to the manufacturer's instructions. These libraries were sequenced on the Illumina sequencing platform HiSeq™ 2500 (Aksomics, Shanghai, China).

Animal experiments

All male BALB/c nude mice (20 ± 2 g) were purchased from Guangdong Medical Laboratory Animal Center (MLAC). All animal experiments were performed in accordance with the principles and procedures outlined in the Gannan Medical University Guide for the Care. Approval was obtained from the the First Affiliated Hospital of Gannan Medical University Animal Ethics Committee.

To observe tumor growth, the transfected cells were injected subcutaneously into the left side of the axilla. Tumor growth was evaluated by detecting the volumes of the xenografts once a week. Specifically, the formula for calculating the volumes was defined: (volume) = 1/2 x (long axis) x (short axis).

To establish a lung metastasis model, cancer cells stably expressing firefly luciferase were injected into 4-week-old BALB/c nude mice from the tail vein. Six weeks after injection, bioluminescent pictures of tumor lung metastases were obtained using an in vivo imaging system. The mice were sacrificed, and the lung tissue of nude mice was taken out to record the number of lung metastases, and histological sections and HE staining were performed.

Statistical analysis

SPSS (version 22.0) and GraphPad Prism 9.1 (GraphPad Software Inc., CA, USA) were used for statistical analysis. Student's t test and/or chi-squared test were statistically employed for data analysis. Results were indicated as mean \pm SD. $P < 0.05$ was considered significant.

Results

Expression and identification of hsa_circ_0021727 in ESCC tissues and cells

To explore the expression of circRNAs in ESCC tissues and paracancerous tissues, three pairs of samples (3 ESCC tissues and 3 paracancerous tissues) were used for circRNA microarray analysis. It was found that 7518 circRNAs were expressed in ESCC tissues and paracancerous tissues. Twenty up-regulated or down-regulated circRNAs were screened, among which hsa_circ_0021727 was the most up-regulated circRNA in cancer tissues compared with normal tissues (Fig. 1A). Volcano plots showed changes in circRNA expression between cancerous and paracancerous tissues (Fig. 1B). Hsa_circ_0021727 is derived from CD44 and is spliced from exon 6 to exon 9. Sanger sequencing confirmed the junction sequence in the divergent primers spanning the predicted products (Fig. 1C). Agarose gel electrophoresis also verified the existence of hsa_circ_0021727 (Fig. 1D). We confirmed the cyclic character of hsa_circ_0021727. First, we digested total RNA with RNaseR. The results showed that hsa_circ_0021727 had stronger RNaseR resistance than linear CD44 (Fig. 1E). Then, we designed random hexamer or oligo(dT)18 primers for qPCR. The relative expression of hsa_circ_0021727 was obviously lower when oligo(dT)18 primers were applied than when random hexamer primers were used, while linear CD44 expression was unchanged (Fig. 1F). FISH results showed that hsa_circ_0021727 was mainly located in the cytoplasm (Fig. 1G). The clinicopathological data of the patients in the tissue microarrays were counted (Table S1A). RNA-ISH revealed that the expression of hsa_circ_0021727 was higher in cancer tissues of ESCC patients than in adjacent tissues (Fig. 1H and I). 54.9% of patients had high expression of hsa_circ_0021727 (Table S1B). The expression of Hsa_circ_0021727 had no statistical significance with the patient's age, clinical analysis, distant metastasis and lymph node metastasis, but was significantly correlated with the patient's survival (Table 1). Cox multivariate analysis showed that the expression of hsa_circ_0021727 had reached a significant difference. The expression of Hsa_circ_0021727 can be used as an independent prognostic factor for patients (Table 2). The survival time of patients with high expression of hsa_circ_0021727 was significantly lower than that of patients with low expression of hsa_circ_0021727 (Fig. 1J).

Hsa_circ_0021727 promotes migration, invasion and proliferation of ESCC cells in vitro

To understand the function of hsa_circ_0021727, we designed overexpression and knockdown lentiviral vectors of hsa_circ_0021727. qRT-PCR examined the efficiency of lentiviral vector transfection (Fig. 2A

and C). The migration ability of ESCC cells was detected by wound healing assays. The results suggested that the migration ability of ESCC cells was enhanced after overexpression of hsa_circ_0021727. In contrast, knockdown of hsa_circ_0021727 inhibited the migration ability of ESCC cells (Fig. 2B and D). The results of transwell assays showed that hsa_circ_0021727 could promote ESCC cell invasion, while hsa_circ_0021727 deficiency inhibited ESCC cell invasion (Fig. 2E). Furthermore, in three-dimensional (3D) spheroid invasion assays, ESCC cells overexpressing hsa_circ_0021727 had more cellular antennae than control cells and displayed morphological changes typical of highly invasive cells. However, this invasion ability of ESCC cells knocked down hsa_circ_0021727 was attenuated (Fig. 2F). The results of MTT assays revealed that cells transfected with the hsa_circ_0021727 overexpressing vector had stronger proliferation ability. After knockdown of hsa_circ_0021727, the proliferation ability of ESCC cells was significantly inhibited (Fig. 2G and H). We also verified the proliferation of ESCC cells by colony clone formation assays. It was found that overexpression of hsa_circ_0021727 promoted cell proliferation, while knockdown of hsa_circ_0021727 inhibited cell proliferation (Fig. 2I). EdU immunofluorescence assays obtained the same results (Fig. 2J). Taken together, these results suggested that hsa_circ_0021727 promoted ESCC cell proliferation, invasion and migration.

Hsa_circ_0021727 promotes metastasis and proliferation of ESCC cells in vivo

To evaluate the effect of hsa_circ_0021727 on proliferation and metastasis in vivo, we performed subcutaneous tumorigenesis and mice tail vein injection assays in BALB/c nude mice. Stably transfected hsa_circ_0021727 overexpressing or knockdown ESCC cells (TE-1) were used for the experiments. For the lung metastasis model, we first observed intravital fluorescence imaging, then sacrificed the mice and examined the formation of metastatic tumor nodules in the lungs. It was found that mice injected with hsa_circ_0021727 overexpressing cells had more metastatic nodules, while mice injected with hsa_circ_0021727 knockdown cells had fewer metastatic nodules (Fig. 3A-D). Subcutaneously injected into BALB/c nude mice were used to assess tumor growth. The results showed that the tumor volume and weight of the hsa_circ_0021727 overexpression group increased significantly, compared to those of the empty vector group. At the same time, the volume and weight of tumors in the hsa_circ_0021727 knockdown group were significantly reduced, compared to those of the scramble group (Fig. 3F and G). We also verified the expression of hsa_circ_0021727 and miR-23b-5p in mouse tumor tissues by qPCR (Fig. 3E). Immunohistochemical analysis showed that the expression of Ki67 and MMP9 in mice tumors was positively correlated with the expression of hsa_circ_0021727 (Fig. 3H).

Hsa_circ_0021727 function as a sponge for miR-23b-5p

CircRNAs acting as sponges for miRNAs have been well reported. To search for miRNAs that may bind to hsa_circ_0021727, we selected five miRNAs (miR-23a-5p, miR-23b-5p, miR-218-5p, miR-433-3p, and miR-494-5p) with the highest scores in the miRanda database (Fig. 4A). We designed biotinylated hsa_circ_0021727 probe and oligo probe. We verified the pull-down efficiency of the hsa_circ_0021727 probe (Fig. 4B). The RNA pull-down results revealed that among the five candidate miRNAs, only miR-23b-5p could be heavily pulled down by the hsa_circ_0021727 probe in ESCC cells transfected with the

hsa_circ_0021727 overexpressing vector(Fig. 4C and D).The qRT-PCR results also confirmed that the expression of hsa_circ_0021727 was negatively correlated with the expression of miR-23b-5p(Fig. 4E and F).To further verify that hsa_circ_0021727 can bind to miR-23b-5p, we first designed a mutant of miR-23b-5p, and then performed luciferase reporter gene analysis.The results showed that miR-23b-5p attenuated luciferase activity, while the miR-23b-5p mutant had no such effect(Fig. 4G).Furthermore, FISH analysis found that hsa_circ_0021727 and miR-23b-5p co-localized in the cytoplasm(Fig. 4H).Overall, these results indicated that hsa_circ_0021727 acts as a sponge for miR-23b-5p.

Hsa_circ_0021727 promotes ESCC cell proliferation, invasion and migration via miR-23b-5p

To investigate the effect of miR-23b-5p on the function of ESCC cells, the miR-23b-5p overexpression vector was used to transfect ESCC cells.For wound healing assay, we found that miR-23b-5p overexpression increased the width of linear wounds.After co-transfection of hsa_circ_0021727 and miR-23b-5p overexpression vectors, miR-23b-5p reduced the migration ability of hsa_circ_0021727(Fig. 5A and B).The results of transwell assays showed that the invasion ability of ESCC cells was weakened after transfection overexpression miR-23b-5p. After co-transfection of hsa_circ_0021727 overexpression vector, miR-23b-5p neutralized the effect of hsa_circ_0021727.(Fig. 5C).This indicated that hsa_circ_0021727 was a negative regulator of miR-23b-5p.We obtained the same trend with three-dimensional (3D) spheroid invasion assays(Fig. 5D).The results of the MTT assays indicated that the proliferation capacity of the cells was enhanced after transfection of miR-23b-5p alone.After co-transfection of hsa_circ_0021727 and miR-23b-5p overexpression vector, miR-23b-5p attenuated the efficiency of hsa_circ_0021727(Fig. 5E and F). Colony formation assays confirmed the same results again(Fig.5G).Our results confirmed that hsa_circ_0021727 could promote ESCC cell proliferation, invasion and migration through miR-23b-5p.

Hsa_circ_0021727 promotes the metastasis and proliferation of ESCC cells in vivo by regulating the expression of miR-23b-5p

ESCC cells were divided into four groups co-transfected with the hsa_circ_0021727 overexpressing vector and miR-23b-5p overexpression vector.The treated ESCC cells were subcutaneously inoculated into BALB/c nude mice.It was found that miR-23b-5p could inhibit tumor growth in vivo. Hsa_circ_0021727 attenuated the effect of miR-23b-5p in vivo(Fig. 6A and B).Four groups of cells were injected into the tail vein of BALB/c nude mice.The results of the lung metastasis model showed that transfection of miR-23b-5p resulted in fewer metastatic nodules in mice.However, after co-transfection of hsa_circ_0021727, metastatic pulmonary nodules were significantly increased.(Fig. 6C and D).We also sectioned and HE stained the metastatic nodules(Fig. 6E).Therefore, we believed that hsa_circ_0021727 promoted the metastasis and proliferation of ESCC cells in vivo via miR-23b-5p.

Hsa_circ_0021727 activates TAB1/NFκB signaling via miR-23b-5p

To determine the downstream pathways regulated by hsa_circ_0021727, we performed transcriptome sequencing using ESCC cells (KYSE-510) transfected with hsa_circ_0021727 overexpression vector and empty vector. Heatmaps revealed the expression of downstream gene (Fig. 7A). The top 20 GO terms of biological process were screened out (Fig. 7B). The results of Gene Set Enrichment Analysis (GSEA) showed that the expression of hsa_circ_0021727 was significantly positively correlated with NFκB signalling (Fig. 7C). qRT-PCR verified that the expression of hsa_circ_0021727 was highly correlated with the downstream factors of NFκB pathway (Fig. 7D and E). In our paper, hsa_circ_0021727 has been shown to act as a sponge for miR-23b-5p. To identify possible target genes of miR-23b-5p in ESCC cells, we used online software (miRanda) to make predictions. We found that miR-23b-5p had a binding site for TAB1. TAB1 is an adaptor protein constitutively associated with N-terminal kinase domain of TAK1 even in the unstimulated cells, while TAB2 and TAB3 bind to the C-terminus of TAK1 through TAK1-binding domain after stimulation [27, 28]. TAB1, TAB2, TAB3 and TAK1 form the TAK1-TABs complex [29]. The TAK1-TABs complex phosphorylates IKKβ at Ser177 and Ser181, which is required for the activation of NF-κB signaling [30, 31]. Through dual luciferase experiments, we found that hsa_circ_0021727 could enhance the luciferase activity of NF-κB (Fig. 7F). Western blot analysis showed that the protein expression of TAB1, p-IKK-B and p-IKBA was up-regulated after overexpression of hsa_circ_0021727. On the contrary, the expression of TAB1, p-IKK-B, p-IKBA was down-regulated after transfection of circ_0021727-shRNA (Fig. 7G). We performed dual luciferase reporter experiments by constructing wildtype (WT) and mutant type (MUT) dual-luciferase reporter vectors (GP-miRGLO) for TAB1 (Fig. 7H). Compared with the NC, the miR-23b-5p significantly reduced the luciferase activity of the WT reporter, while the miR-27a-3p did not affect the luciferase activity of the MUT reporter (Fig. 7I). Furthermore, knockdown of hsa_circ_0021727 reduced luciferase activity, whereas hsa_circ_0021727 did not affect the luciferase activity of the MUT reporter gene (Fig. 7J). To explore the relationship between hsa_circ_0021727, miR-23b-5p and TAB1, we selected 8 ESCC patient specimens for qRT-PCR and western blot. The results revealed that hsa_circ_0021727 was negatively correlated with the expression of miR-23b-5p, but positively correlated with the expression of TAB1 (Fig. 7K and L). N-(4-Ethylphenyl)-N'-phenylurea (INH14) reduced NF-κB activation by inhibiting IKK [32]. We can block the NFκB pathway by adding INH14. Through western blot analysis, we found that miR-23b-5p could downregulate TAB1 expression, while co-transfection of hsa_circ_0021727 neutralized this effect. At the same time, the expression of TAB1 was not affected by INH14 (Fig. 7N). This indicates that the expression of TAB1 was regulated by both hsa_circ_0021727 and miR-23b-5p. We also found that the expressions of CyclinD1, MMP2 and MMP9 were positively regulated by hsa_circ_0021727 and negatively regulated by miR-23b-5p. However, the expression of P21 is just the opposite (Fig. 7N). Knockdown of TAB1 inhibited the proteins expression of CyclinD1, MMP2, MMP9 and NF-κB (Fig. 7M). This suggests that these factors were not only regulated by hsa_circ_0021727 but also by TAB1. In general, hsa_circ_0021727 can activate TAB1/NFκB signaling via miR-23b-5p.

Hsa_circ_0021727 promotes ESCC cell proliferation, invasion and migration by activating the TAB1/NFκB pathway

To investigate the effect of TAB1 on the function of ESCC cells, the TAB1 knockdown plasmid and hsa_circ_0021727 overexpression vector were transfected into ESCC cells. For wound healing experiments, we found that knockdown of TAB1 increased the width of linear wounds (Fig. 8A and C). After the addition of INH14, the migration ability of ESCC cells was inhibited (Fig. 8B and D). The results of transwell assay showed that the invasive ability of ESCC cells was weakened after transfection with TAB1 knockdown plasmid (Fig. 8E). The addition of INH14 on the basis of overexpression hsa_circ_0021727 also attenuated the invasion ability of ESCC cells (Fig. 8F). We obtained the same trend with three-dimensional (3D) spheroid invasion assays (Fig. 8G and H). The results of MTT experiments indicated that TAB1 attenuated the ability of hsa_circ_0021727 after co-transfection of hsa_circ_0021727 overexpression vector and TAB1 knockdown plasmid (Fig. 8I and J). INH14 also inhibited the ability of hsa_circ_0021727 (Fig. 8K and L). We verified the same results by colony formation assays (Fig. 8M and N). In short, hsa_circ_0021727 promotes ESCC cell proliferation, invasion and migration by activating the TAB1/NFκB pathway.

Discussion

Esophageal cancer is characterized by high morbidity and mortality in China, ranking sixth in incidence and fifth in mortality [33]. Factors such as hot diet and long-term nitrite intake increase the incidence of esophageal squamous cell carcinoma [34, 35]. ESCC is difficult to detect in the early stage, and the treatment effect is extremely poor. With more and more people dying from ESCC, the search for a new biomarker and target has become an urgent issue. In this study, we discovered a novel circRNA, which can serve as a potential biomarker and target for the early diagnosis and treatment of ESCC.

It has been widely reported that circRNAs play an important role in cancer. Its earliest discovered function is to negatively regulate miRNAs through "sponge adsorption". For example, hsa_circ_001783 promoted progression of breast cancer cells via sponging miR-200c-3p [36]. Circular RNA circSLC8A1 acts as a sponge of miR-130b/miR-494 in suppressing bladder cancer progression via regulating PTEN [37]. CircRNAs can also function through exosomes. Exosomal circSHKBP1 promotes gastric cancer progression via regulating the miR-582-3p/HUR/VEGF axis and suppressing HSP90 degradation [38]. CircRNAs have been found to be involved in the regulation of certain protein-protein and protein-RNA interactions [39]. CircDCUN1D4 directly interacts with TXNIP mRNA through base complementation, thereby stabilizing TXNIP expression and inhibiting tumor metastasis and glycolysis in lung adenocarcinoma [40]. CircRNAs also were confirmed to have the function of being translated into polypeptides. Circ-ZNF609 was found to associate with heavy polysomes, and it is translated into a protein in a splicing-dependent and cap-independent manner, providing an example of a protein-coding circRNA in eukaryotes [41]. N6-methyladenosine modification is a way for circRNAs to exert their

functions. N⁶-methyladenosine modification of circNSUN2 facilitates cytoplasmic export and stabilizes HMGA2 to promote colorectal liver metastasis[42]. In our study, we found that the expression of hsa_circ_0021727 was increased in ESCC patients and was highly correlated with the prognosis of ESCC patients. Hsa_circ_0021727 could promote the proliferation, invasion and migration of ESCC cells. Hsa_circ_0021727 may serve as a diagnostic marker and potential therapeutic target for ESCC.

MicroRNA is a non-coding RNA of about 22 nucleotides in length. It was first thought to bind to the 3' UTR of gene mRNA by incomplete complementation, inhibiting protein translation, thereby inhibiting protein synthesis and blocking the translation process of mRNA. Typically, miRNAs negatively regulate target genes and can degrade mRNA or inhibit translation. At the same time, MicroRNAs also play an important role in the occurrence and development of tumors. For instance, microRNA-106a regulates autophagy-related cell death and EMT by targeting TP53INP1 in lung cancer with bone metastasis[43]. Tumor-derived exosomal miR-934 induces macrophage M2 polarization to promote liver metastasis of colorectal cancer[44]. Studies have shown that circRNA may have a base sequence that binds to miRNA, which can act as a competitive endogenous RNA to competitively bind to miRNA, relieve the inhibitory effect of miRNA on target genes, and then affect the occurrence and development of tumors[45]. Circ-ZEB1 promotes PIK3CA expression by silencing miR-199a-3p and affects the proliferation and apoptosis of hepatocellular carcinoma[46]. Our previous experiments found that hsa_circ_0021727 could act as a "molecular sponge" for miR-23b-5p. MiR-23b-5p was shown to be an important regulatory molecule in tumorigenesis and development. Dysregulation of miR-23b-5p promotes cell proliferation via targeting FOXM1 in hepatocellular carcinoma[47]. MiR-23b-5p promotes the chemosensitivity of temozolomide via negatively regulating TLR4 in glioma[48]. In our experiments, miR-23b-5p played an important role as a tumor suppressor. It can reduce the translation of the downstream target gene TAB1, thereby inactivating the NF κ B pathway.

Table 1 was shown to be an adaptor protein that can bind to TAK1 to change its structure and activate TAK1[49]. TAK1 is a member of the protein kinase complex consisting of TAK1, TAB1 and TAB2 that phosphorylate IKK2 and NIK. The TAK1-TABs complex phosphorylates IKK β at Ser177 and Ser181, which is required for activation of NF- κ B signaling[50]. Therefore, TAB1 and TAK1 are key regulators of NF- κ B activation. NF- κ B is an important intracellular nuclear transcription factor, which has five members, including NF- κ B1 (p50), NF- κ B2 (p52), RelA (p65), RelB and c-Rel[51]. Both TAK1-TABs complex and NF- κ B are considered to be highly tumor-related factors. It was shown that TAB1 promoted cell proliferation, invasion and migration in non-small cell lung cancer[52]. TAB1 regulated papillary thyroid cancer cell proliferation and migration[53]. Santoro et al. identified TAK1 as a central hub integrating the most relevant signals sustaining pancreatic cancer aggressiveness and chemoresistance[54]. Tan et al. found that specific deletion of TAK1 in hepatocytes promoted liver fibrosis and hepatocellular carcinoma[55]. Aberrant activation of TAK1-TABs complex activates NF- κ B signaling to promote tumor progression. For example, studies have shown that activation of the TAB1/TAK1/IKK β /NF- κ B signaling axis by TGF- β is a key factor in breast cancer cell invasion[56]. In this paper, our results showed that TAB1 was positively correlated with the expression of hsa_circ_0021727 and negatively correlated with the

expression of miR-23b-5p. Activation of the TAB1/TAK1/IKK β /NF- κ B signaling axis induced proliferation, invasion and migration of ESCC cells.

Conclusion

In conclusion, our study identified a novel circRNA (hsa_circ_0021727) that was aberrantly expressed in ESCC patients. The previous findings indicated that hsa_circ_0021727 could promote the proliferation, invasion and migration of ESCC cells. More critically, hsa_circ_0021727 acted by "sponge adsorption" of miR-23b-5p to activate the TAB1/NF- κ B pathway (Fig. 9). Our work elucidates the mechanism of hsa_circ_0021727 in ESCC, which provides biomarkers and potential targets for ESCC diagnosis and therapy.

Abbreviations

circRNA: Circular RNA; ESCC: esophageal squamous cell carcinoma;

ncRNAs: non-coding RNAs; miRNAs: microRNAs;

RNA-ISH: CircRNA in situ hybridization;

qRT-PCR: Total RNA extraction and quantitative real-time PCR;

FISH: Fluorescence in situ hybridization; EdU: 5-Ethynyl-2'-deoxyuridine;

MTT: 3-[4,5-Dimethylthiazol-2-yl]-2,5-diphenyltetrazolium;

3D: bromide; three-dimensional; GSEA : Gene Set Enrichment Analysis;

TAB1: TAK1-binding protein 1; INH14: N-(4-Ethylphenyl)-N'-phenylurea;

WT: wildtype; MUT: mutant type.

Declarations

Acknowledgements

Not applicable.

Authors' contributions

XH, FM and XKZ designed experiments and proposed hypotheses. XH, FM, XKZ and YTW completed in vitro experiments. JL, YTW and YLT completed in vivo experiments. GSZ and BQQ completed the mapping and statistics. XDZ and WYL completed pathological specimen collection and disposal. XH and FM completed the writing of the manuscript. All authors read and approved the final manuscript.

Funding

This research was supported in part by the National Natural Science Foundation of China (81960438 and 82103067) and the National Natural Science Foundation of Jiangxi Province(20202BABL216055 and 20212BAB206078) .

Availability of data and materials

The datasets used and/or analysed during the current study are available from the corresponding author on reasonable request.

Ethics approval and consent to participate

All participants provided written informed consent, and the study was approved by the ethics committee of The First Affiliated Hospital of Gannan Medical University. All animal experiments complied with the Policy of Gannan Medical University on the Care and Use of Laboratory Animals.

Consent for publication

Not applicable.

Competing interests

The authors declare that they have no competing interests.

References

1. Xu J, Pan HW, Wang XQ, Chen KP. Status of diagnosis and treatment of esophageal cancer and non-coding RNA correlation research: a narrative review. *Transl Cancer Res.* 2021;10(10):4532–4552.
2. Siegel RL, Miller KD, Jemal A. Cancer statistics, 2020. *CA Cancer J Clin.* 2020;70(1):7–30.
3. He Z, Ke Y. Precision screening for esophageal squamous cell carcinoma in China. *Chin J Cancer Res.* 2020;32(6):673–682.
4. Matsueda K, Ishihara R. Preoperative Diagnosis and Indications for Endoscopic Resection of Superficial Esophageal Squamous Cell Carcinoma. *J Clin Med.* 2020;10(1):13.
5. Chen W, Zheng R, Baade PD, Zhang S, Zeng H, Bray F, Jemal A, Yu XQ, He J. Cancer statistics in China, 2015. *CA Cancer J Clin.* 2016;66(2):115–32.
6. Uhlenhopp DJ, Then EO, Sunkara T, Gaduputi V. Epidemiology of esophageal cancer: update in global trends, etiology and risk factors. *Clin J Gastroenterol.* 2020;13(6):1010–1021.
7. Lin S, Xu G, Chen Z, Liu X, Li J, Ma L, Wang X. Tea drinking and the risk of esophageal cancer: focus on tea type and drinking temperature. *Eur J Cancer Prev.* 2020;29(5):382–387.
8. Rao W, Lin Z, Liu S, Zhang Z, Xie Q, Chen H, Lin X, Chen Y, Yang H, Yu K, Hu Z. Association between alcohol consumption and oesophageal microbiota in oesophageal squamous cell carcinoma. *BMC*

- Microbiol. 2021;21(1):73.
9. Morselli M, Dieci G. Epigenetic regulation of human non-coding RNA gene transcription. *Biochem Soc Trans.* 2022;BST20210860.
 10. Toden S, Goel A. Non-coding RNAs as liquid biopsy biomarkers in cancer. *Br J Cancer.* 2022;126(3):351–360.
 11. Wang J, Yue BL, Huang YZ, Lan XY, Liu WJ, Chen H. Exosomal RNAs: Novel Potential Biomarkers for Diseases-A Review. *Int J Mol Sci.* 2022;23(5):2461.
 12. Min X, Liu DL, Xiong XD. Circular RNAs as Competing Endogenous RNAs in Cardiovascular and Cerebrovascular Diseases: Molecular Mechanisms and Clinical Implications. *Front Cardiovasc Med.* 2021;8:682357.
 13. Patil NS, Feng B, Su Z, Castellani CA, Chakrabarti S. Circular RNA mediated gene regulation in chronic diabetic complications. *Sci Rep.* 2021;11(1):23766.
 14. Gong W, Xu J, Wang Y, Min Q, Chen X, Zhang W, Chen J, Zhan Q. Nuclear genome-derived circular RNA circPUM1 localizes in mitochondria and regulates oxidative phosphorylation in esophageal squamous cell carcinoma. *Signal Transduct Target Ther.* 2022;7(1):40.
 15. Liu Z, Gu S, Wu K, Li L, Dong C, Wang W, Zhou Y. CircRNA-DOPEY2 enhances the chemosensitivity of esophageal cancer cells by inhibiting CPEB4-mediated Mcl-1 translation. *J Exp Clin Cancer Res.* 2021;40(1):361.
 16. Zhou PL, Wu Z, Zhang W, Xu M, Ren J, Zhang Q, Sun Z, Han X. Circular RNA hsa_circ_0000277 sequesters miR-4766-5p to upregulate LAMA1 and promote esophageal carcinoma progression. *Cell Death Dis.* 2021;12(7):676.
 17. Hu X, Wu D, He X, Zhao H, He Z, Lin J, Wang K, Wang W, Pan Z, Lin H, Wang M. circGSK3 β promotes metastasis in esophageal squamous cell carcinoma by augmenting β -catenin signaling. *Mol Cancer.* 2019;18(1):160.
 18. Hansen TB, Jensen TI, Clausen BH, Bramsen JB, Finsen B, Damgaard CK, Kjems J. Natural RNA circles function as efficient microRNA sponges. *Nature.* 2013;495(7441):384–8.
 19. Chen L, Shan G. CircRNA in cancer: Fundamental mechanism and clinical potential. *Cancer Lett.* 2021;505:49–57.
 20. Landskroner-Eiger S, Moneke I, Sessa WC. miRNAs as modulators of angiogenesis. *Cold Spring Harb Perspect Med.* 2013;3(2):a006643.
 21. Pal AS, Kasinski AL. Animal Models to Study MicroRNA Function. *Adv Cancer Res.* 2017;135:53–118.
 22. Galagali H, Kim JK. The multifaceted roles of microRNAs in differentiation. *Curr Opin Cell Biol.* 2020;67:118–140.
 23. Yang H, Fang X, Shen Y, Yao W, Chen D, Shen L. MiR-153-3p reduces extracellular matrix accumulation in high glucose-stimulated human glomerular mesangial cells via targeting PAQR3 in diabetic nephropathy. *Endocrinol Diabetes Nutr (Engl Ed).* 2022;69(1):34–42.

24. Zhu L, Yang Y, Li H, Xu L, You H, Liu Y, Liu Z, Liu X, Zheng D, Bie J, Li J, Song C, Yang B, Luo J, Chang Q. Exosomal microRNAs induce tumor-associated macrophages via PPAR γ during tumor progression in SHH medulloblastoma. *Cancer Lett.* 2022;215630.
25. Wu S, Liu S, Cao Y, Chao G, Wang P, Pan H. Downregulation of ZC3H13 by miR-362-3p/miR-425-5p is associated with a poor prognosis and adverse outcomes in hepatocellular carcinoma. *Aging (Albany NY).* 2022;14(undefined).
26. Yang H, Li X, Meng Q, Sun H, Wu S, Hu W, Liu G, Li X, Yang Y, Chen R. CircPTK2 (hsa_circ_0005273) as a novel therapeutic target for metastatic colorectal cancer. *Mol Cancer.* 2020;19(1):13.
27. Shibuya H, Yamaguchi K, Shirakabe K, Tonegawa A, Gotoh Y, Ueno N, Irie K, Nishida E, Matsumoto K. TAB1: an activator of the TAK1 MAPKKK in TGF-beta signal transduction. *Science (1996)* 272:1179–82.
28. Xu YR, Lei CQ. TAK1-TABs Complex: A Central Signalosome in Inflammatory Responses. *Front Immunol.* 2021;11:608976.
29. Besse A, Lamothe B, Campos AD, Webster WK, Maddineni U, Lin SC, Wu H, Darnay BG. TAK1-dependent signaling requires functional interaction with TAB2/TAB3. *J Biol Chem (2007)* 282:3918–28.
30. Zandi E, Rothwarf DM, Delhase M, Hayakawa M, Karin M. The I κ B kinase complex (IKK) contains two kinase subunits, IKK α and IKK β , necessary for I κ B phosphorylation and NF- κ B activation. *Cell (1997)* 91:243–52.
31. Wang S, Li H, Chen R, Jiang X, He J, Chaozheng L. TAK1 confers antibacterial protection through mediating the activation of MAPK and NF- κ B pathways in shrimp. *Fish Shellfish Immunol.* 2022;S1050-4648(22)00134-6.
32. Drexel M, Kirchmair J, Santos-Sierra S. INH14, a Small-Molecule Urea Derivative, Inhibits the IKK α / β -Dependent TLR Inflammatory Response. *Chembiochem.* 2019;20(5):710–717.
33. Qiu H, Cao S, Xu R. Cancer incidence, mortality, and burden in China: a time-trend analysis and comparison with the United States and United Kingdom based on the global epidemiological data released in 2020. *Cancer Commun (Lond).* 2021;41(10):1037–1048.
34. Abnet CC, Arnold M, Wei WQ. Epidemiology of Esophageal Squamous Cell Carcinoma. *Gastroenterology.* 2018;154(2):360–373.
35. Yang J, Liu X, Cao S, Dong X, Rao S, Cai K. Understanding Esophageal Cancer: The Challenges and Opportunities for the Next Decade. *Front Oncol.* 2020;10:1727.
36. Liu Z, Zhou Y, Liang G, Ling Y, Tan W, Tan L, Andrews R, Zhong W, Zhang X, Song E, Gong C. Circular RNA hsa_circ_001783 regulates breast cancer progression via sponging miR-200c-3p. *Cell Death Dis.* 2019;10(2):55.
37. Lu Q, Liu T, Feng H, Yang R, Zhao X, Chen W, Jiang B, Qin H, Guo X, Liu M, Li L, Guo H. Circular RNA circSLC8A1 acts as a sponge of miR-130b/miR-494 in suppressing bladder cancer progression via regulating PTEN. *Mol Cancer.* 2019;18(1):111.

38. Xie M, Yu T, Jing X, Ma L, Fan Y, Yang F, Ma P, Jiang H, Wu X, Shu Y, Xu T. Exosomal circSHKBP1 promotes gastric cancer progression via regulating the miR-582-3p/HUR/VEGF axis and suppressing HSP90 degradation. *Mol Cancer*. 2020;19(1):112.
39. Huang A, Zheng H, Wu Z, Chen M, Huang Y. Circular RNA-protein interactions: functions, mechanisms, and identification. *Theranostics*. 2020;10(8):3503–3517.
40. Liang Y, Wang H, Chen B, Mao Q, Xia W, Zhang T, Song X, Zhang Z, Xu L, Dong G, Jiang F. circDCUN1D4 suppresses tumor metastasis and glycolysis in lung adenocarcinoma by stabilizing TXNIP expression. *Mol Ther Nucleic Acids*. 2020;23:355–368.
41. Legnini I, Di Timoteo G, Rossi F, Morlando M, Briganti F, Sthandier O, Fatica A, Santini T, Andronache A, Wade M, Laneve P, Rajewsky N, Bozzoni I. Circ-ZNF609 Is a Circular RNA that Can Be Translated and Functions in Myogenesis. *Mol Cell*. 2017;66(1):22–37.e9.
42. Chen RX, Chen X, Xia LP, Zhang JX, Pan ZZ, Ma XD, Han K, Chen JW, Judde JG, Deas O, Wang F, Ma NF, Guan X, Yun JP, Wang FW, Xu RH, Dan Xie. N⁶-methyladenosine modification of circNSUN2 facilitates cytoplasmic export and stabilizes HMGA2 to promote colorectal liver metastasis. *Nat Commun*. 2019;10(1):4695.
43. Han L, Huang Z, Liu Y, Ye L, Li D, Yao Z, Wang C, Zhang Y, Yang H, Tan Z, Tang J, Yang Z. MicroRNA-106a regulates autophagy-related cell death and EMT by targeting TP53INP1 in lung cancer with bone metastasis. *Cell Death Dis*. 2021;12(11):1037.
44. Zhao S, Mi Y, Guan B, Zheng B, Wei P, Gu Y, Zhang Z, Cai S, Xu Y, Li X, He X, Zhong X, Li G, Chen Z, Li D. Tumor-derived exosomal miR-934 induces macrophage M2 polarization to promote liver metastasis of colorectal cancer. *J Hematol Oncol*. 2020;13(1):156.
45. Chan JJ, Tay Y. Noncoding RNA: RNA Regulatory Networks in Cancer. *Int J Mol Sci*. 2018;19(5):1310.
46. Liu W, Zheng L, Zhang R, Hou P, Wang J, Wu L, Li J. Circ-ZEB1 promotes PIK3CA expression by silencing miR-199a-3p and affects the proliferation and apoptosis of hepatocellular carcinoma. *Mol Cancer*. 2022;21(1):72.
47. Yang X, Yang S, Song J, Yang W, Ji Y, Zhang F, Rao J. Dysregulation of miR-23b-5p promotes cell proliferation via targeting FOXM1 in hepatocellular carcinoma. *Cell Death Discov*. 2021;7(1):47.
48. Gao K, Wang T, Qiao Y, Cui B. miR-23b-5p promotes the chemosensitivity of temozolomide via negatively regulating TLR4 in glioma. *Acta Biochim Biophys Sin (Shanghai)*. 2021;53(8):979–987.
49. Cheung PC, Nebreda AR, Cohen P. TAB3, a new binding partner of the protein kinase TAK1. 2004;378(Pt 1):27–34.
50. Wang C, Deng L, Hong M, Akkaraju GR, Inoue J, Chen ZJ. TAK1 is a ubiquitin-dependent kinase of MKK and IKK. *Nature*. 2001;412(6844):346–51.
51. Mitchell S, Vargas J, Hoffmann A. Signaling via the NFκB system. *Wiley Interdiscip Rev Syst Biol Med*. 2016;8(3):227–41.
52. Dong Z, Li B, Wang X. MicroRNA-889 plays a suppressive role in cell proliferation and invasion by directly targeting TAB1 in non-small cell lung cancer. *Mol Med Rep*. 2019;20(1):261–269.

53. Chen J, Xu Z, Yu C, Wu Z, Yin Z, Fang F, Chen B. MiR-758-3p regulates papillary thyroid cancer cell proliferation and migration by targeting TAB1. *Pharmazie*. 2019;74(4):235–238.
54. Santoro R, Zanotto M, Simionato F, Zecchetto C, Merz V, Cavallini C, Piro G, Sabbadini F, Boschi F, Scarpa A, Melisi D. Modulating TAK1 Expression Inhibits YAP and TAZ Oncogenic Functions in Pancreatic Cancer. *Mol Cancer Ther*. 2020;19(1):247–257.
55. Tan S, Zhao J, Sun Z, Cao S, Niu K, Zhong Y, Wang H, Shi L, Pan H, Hu J, Qian L, Liu N, Yuan J. Hepatocyte-specific TAK1 deficiency drives RIPK1 kinase-dependent inflammation to promote liver fibrosis and hepatocellular carcinoma. *Proc Natl Acad Sci U S A*. 2020;117(25):14231–14242.
56. Neil JR, Schiemann WP. Altered TAB1:IKK Interaction Promotes TGF- β -Mediated NF- κ B Activation During Breast Cancer Progression. *Cancer Res*. 2008;68(5):1462–70.

Tables

Table 1. Correlation between circ_0021727 expression and clinicopathological characteristics of esophageal cancer

Characteristics		circ_0021727		Chi-square test <i>P</i> -value	Fisher's Exact test <i>P</i> -value
		Low No. cases	High No. cases		
Age (years)	> 55	63	69	0.109	0.109
	≤ 55	10	20		
AJCC clinical stage	I~II	40	39	0.109	0.109
	III~IV	33	50		
T classification	T1~T2	11	17	0.322	0.322
	T3~T4	62	72		
N classification	N0	40	38	0.084	0.084
	N1~N3	33	51		
M classification	No	73	87	0.300	0.300
	Yes	0	2		
Gender	Male	63	77	0.573	0.573
	Female	10	12		
Survive or Mortality	Survive	44	39	0.027	0.027
	Mortality	29	50		

Table 2. Univariate and multivariate analyses of various prognostic parameters in patients with esophageal cancer by cox-regression analysis

	Univariate analysis			Multivariate analysis		
	No. patients	<i>P</i>	Relative risk	<i>P</i>	Relative risk	95% confidence interval
M stage						
M0	160	0.001	10.982	0.012	6.841	1.538-30.430
M1	2					
AJCC stage						
I~II	79	0.002	2.102	0.003	2.035	1.277-3.243
III~IV	83					
Expression of circ00212727						
Low expression	73	0.027	1.679	0.041	1.620	1.021-2.572
High expression	89					

Figures

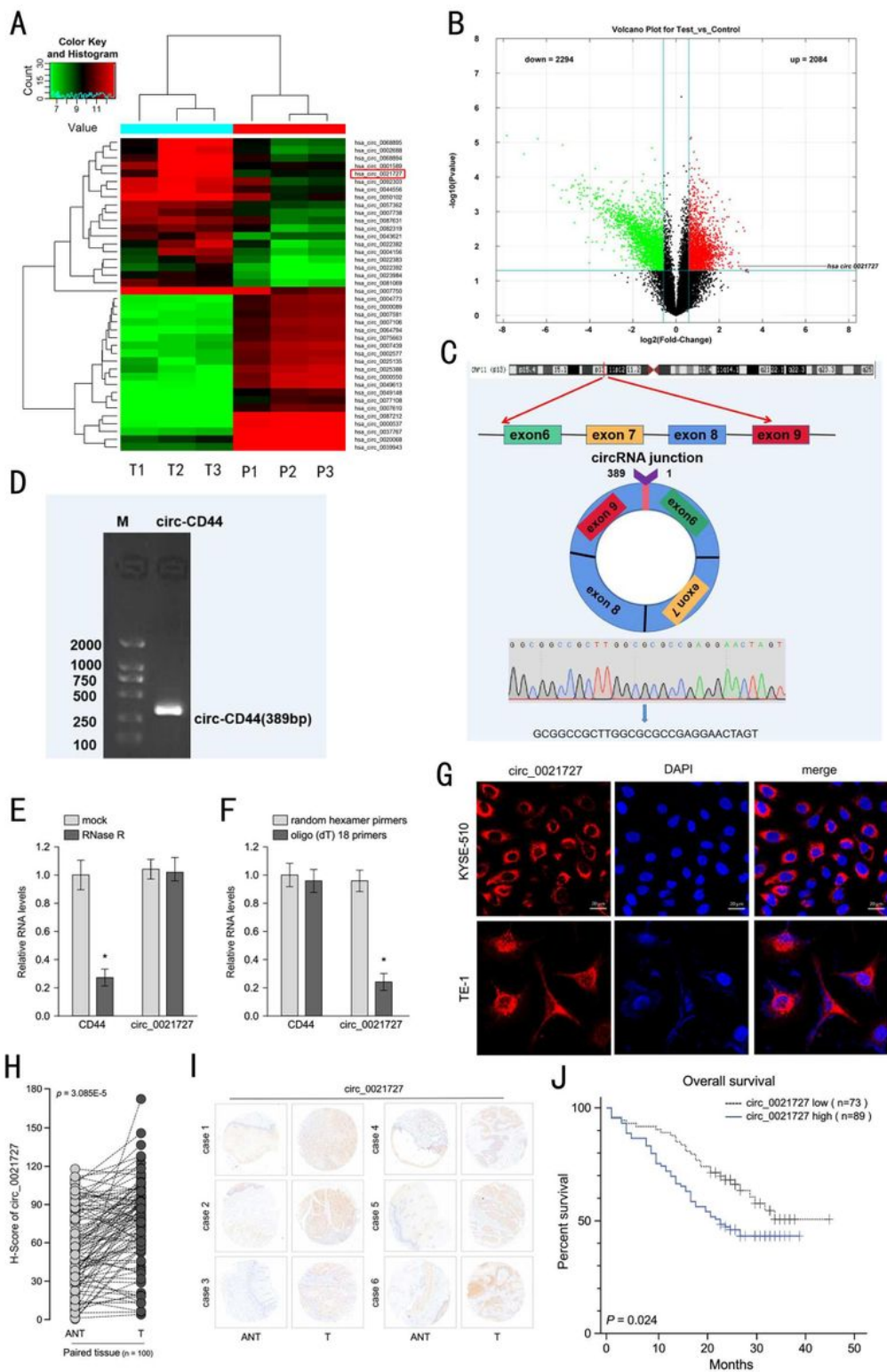


Figure 1

Expression and identification of hsa_circ_0021727. **A** Heat maps of differentially expressed circRNAs in three ESCC tissues (T) and adjacent normal tissues (P). **B** Volcano plots showed changes in circRNA expression between cancerous and paracancerous tissues. **C** Schematic and sanger sequencing of hsa_circ_0021727. **D** Agarose gel electrophoresis detected hsa_circ_0021727 in KYSE 510 cells. **E** The relative RNA levels were examined by RT-qPCR after treatment with RNase R or mock in total RNAs

derived from KYSE 510 cells. **F** Random hexamer or oligo (dT)18 primers were utilized for reverse transcription assays. The relative RNA levels were examined by RT-qPCR and normalized to those generated using random hexamer primers. **G** The subcellular localization of hsa_circ_0021727 in KYSE510 and TE-1 cells performed with FISH. **H** and **I** RNA-ISH detected the expression of hsa_circ_0021727 in ESCC tissues and adjacent tissues. **J** Kaplan–Meier analysis of the OS rates in 162 ESCC patients with high or low expression of hsa_circ_0021727. (Values are expressed as the means \pm SDs; *P < 0.05)

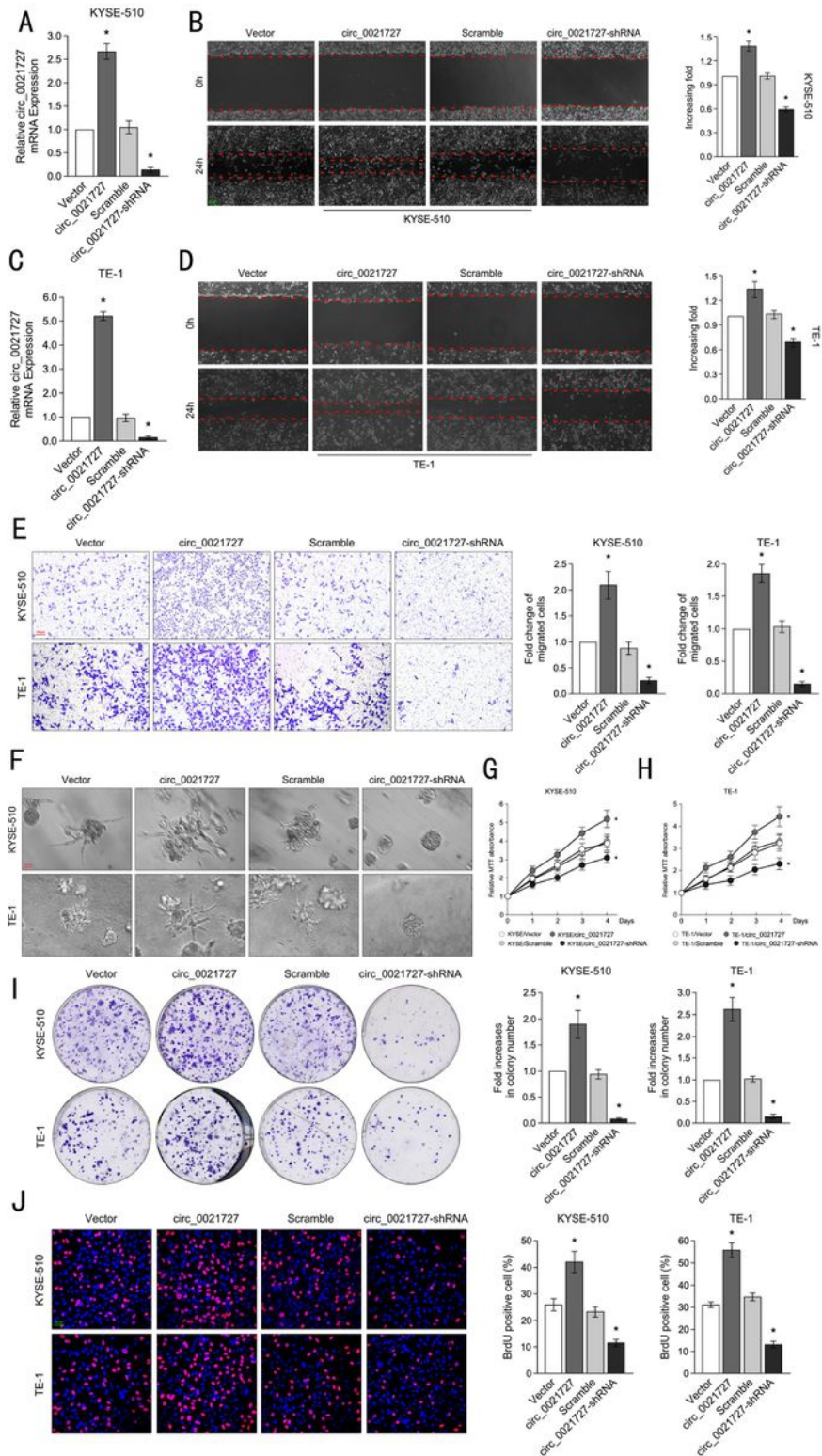


Figure 2

Hsa_circ_0021727 promotes migration, invasion and proliferation of ESCC cells in vitro. **A** and **C** RT-qPCR detected the expression efficiency of hsa_circ_0021727 after cell transfection. **B** and **D** Wound healing assays examined the migration ability of KYSE510 and TE-1 cells after cell transfection. **E** Transwell assays examined the invasive ability of KYSE510 and TE-1 cells after transfection of hsa_circ_0021727 overexpression or knockdown vector. **F** Three-dimensional (3D) spheroid invasion assays showed the effects of hsa_circ_0021727 on the growing antennae of KYSE510 and TE-1 cells. **G** and **H** MTT assays detected the proliferation of KYSE510 and TE-1 cells after transfection of hsa_circ_0021727 overexpression or knockdown vector. **I** Colony formation assays examined the proliferative capacity of KYSE510 and TE-1 cells transfected with hsa_circ_0021727 overexpression or knockdown lentiviral vector. **J** EdU immunofluorescence assays detected the proliferative capacity of KYSE510 and TE-1 cells. (Values are expressed as the means \pm SDs; * $P < 0.05$)

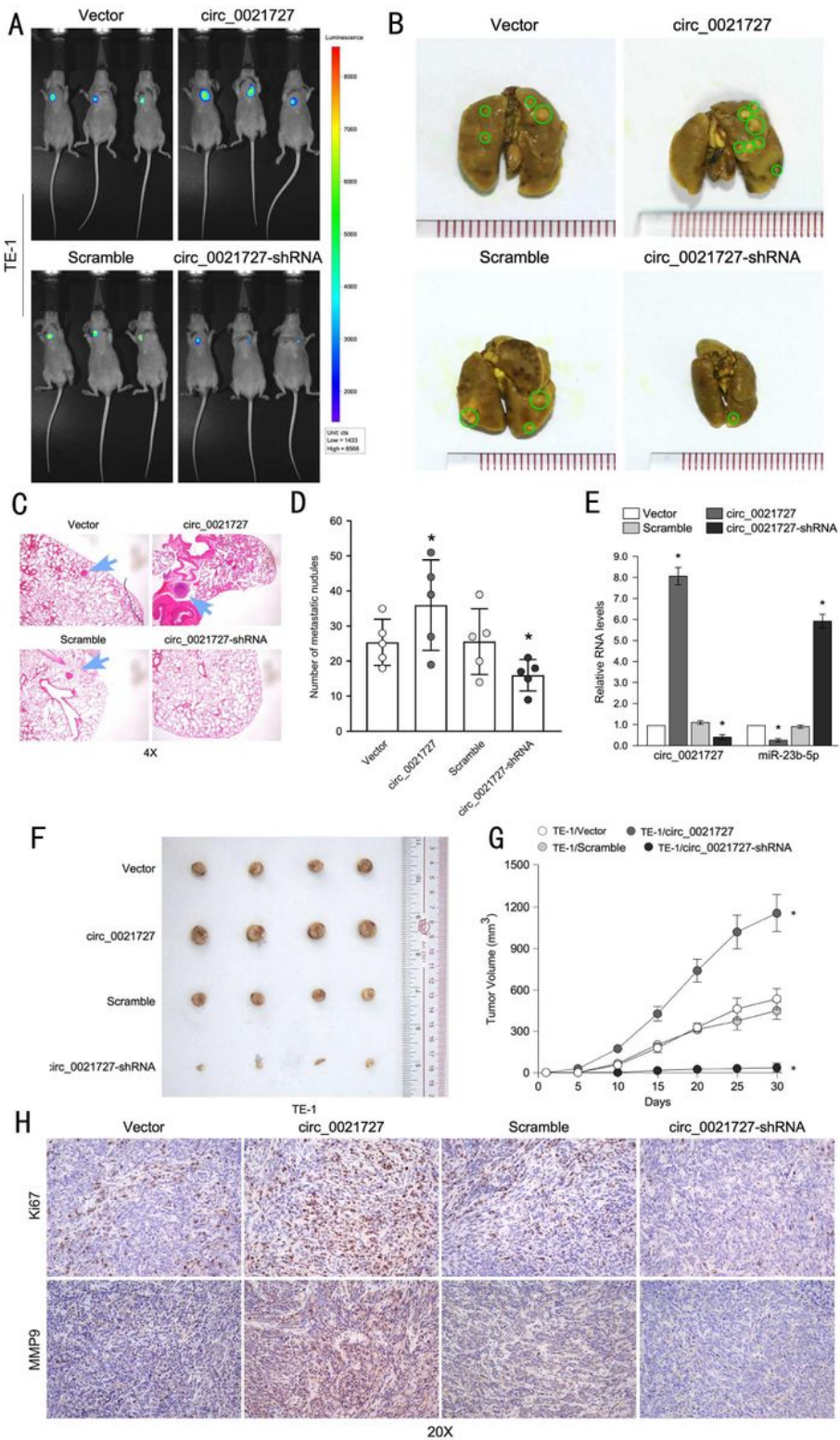


Figure 3

Hsa_circ_0021727 promotes metastasis and proliferation of ESCC cells in vivo. **A** Representative images and analysis of luminescence intensity in tail vein tumor metastasis mouse models. **B** Images of lung tissue in tail vein tumor metastasis mouse models. **C** Lung tissue was stained with HE. **D** Statistical analysis of lung metastatic nodules. **E** qRT-PCR detected the expression hsa_circ_0021727 and miR-23b-5p in mouse tumor tissues. **F** Representative picture of subcutaneous xenograft tumors. **G** Curves of tumor

volumes in subcutaneous xenograft tumors models. **H** Immunohistochemistry showed the expression of Ki67 and MMP9 in mouse tumor tissues. (Values are expressed as the means \pm SDs; *P < 0.05)

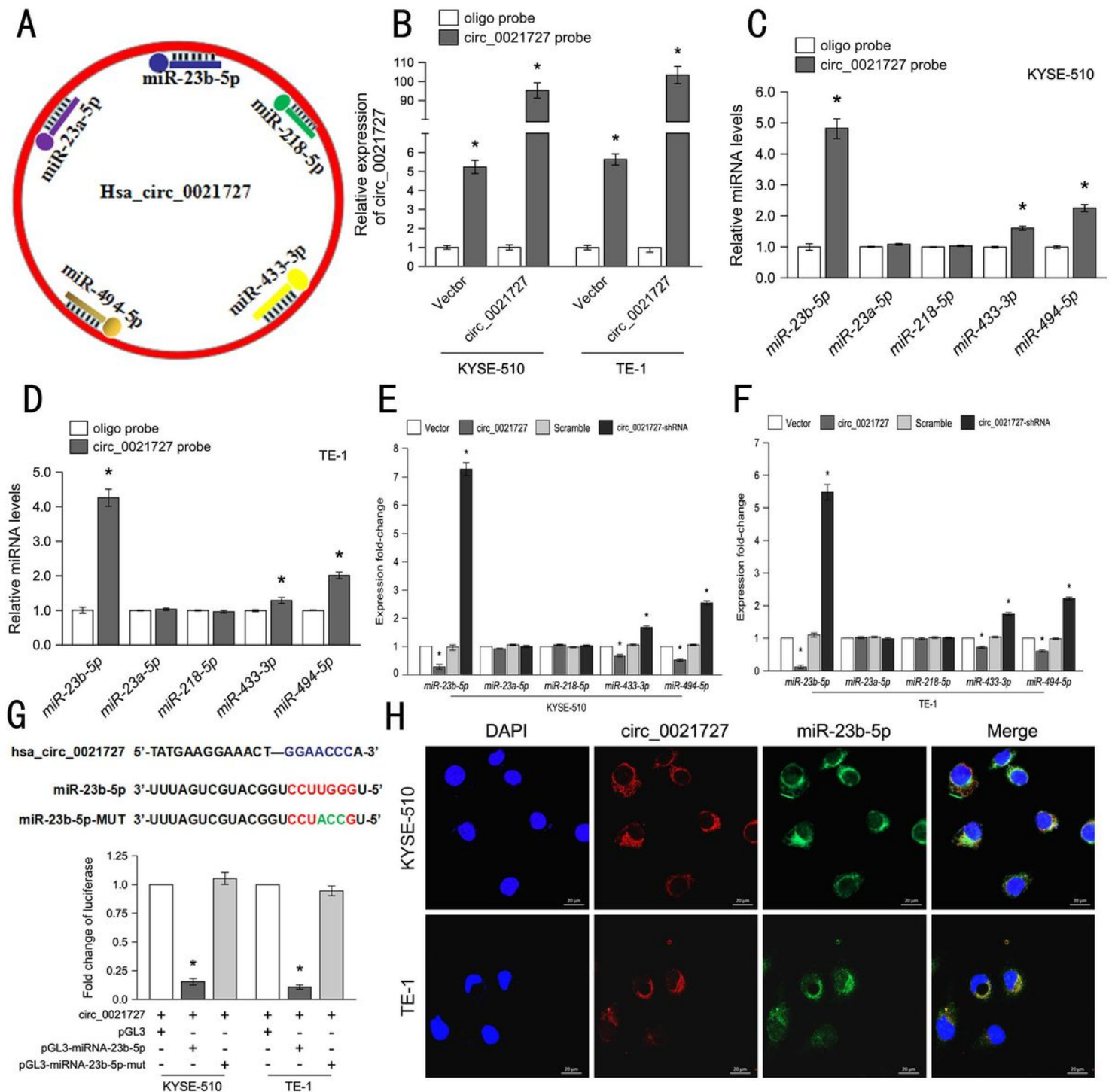


Figure 4

Hsa_circ_0021727 function as a sponge for miR-23b-5p. **A** The picture suggested that hsa_circ_0021727 may target bound miRNAs. **B** Probe efficiency for qRT-PCR detection. **C** and **D** Relative levels of five miRNAs in KYSE510 and TE-1 cells lysates pulled down by hsa_circ_0021727 probe or oligo probe. **E** and

F qRT-PCR detected five miRNA levels in KYSE510 and TE-1 cells transfected with hsa_circ_0021727 overexpression or knockdown lentiviral vector. **G** The luciferase reporter gene assay was performed in KYSE510 and TE-1 cells co-transfected with hsa_circ_0021727 overexpression vector, pGL3 plasmid, pGL3-miR-23b-5p-wt, pGL3-miR-23b-5p-mut. **H** FISH showed the colocalization between hsa_circ_0021727 and miR-23b-5p in KYSE510 and TE-1 cells. (Values are expressed as the means \pm SDs; *P < 0.05)

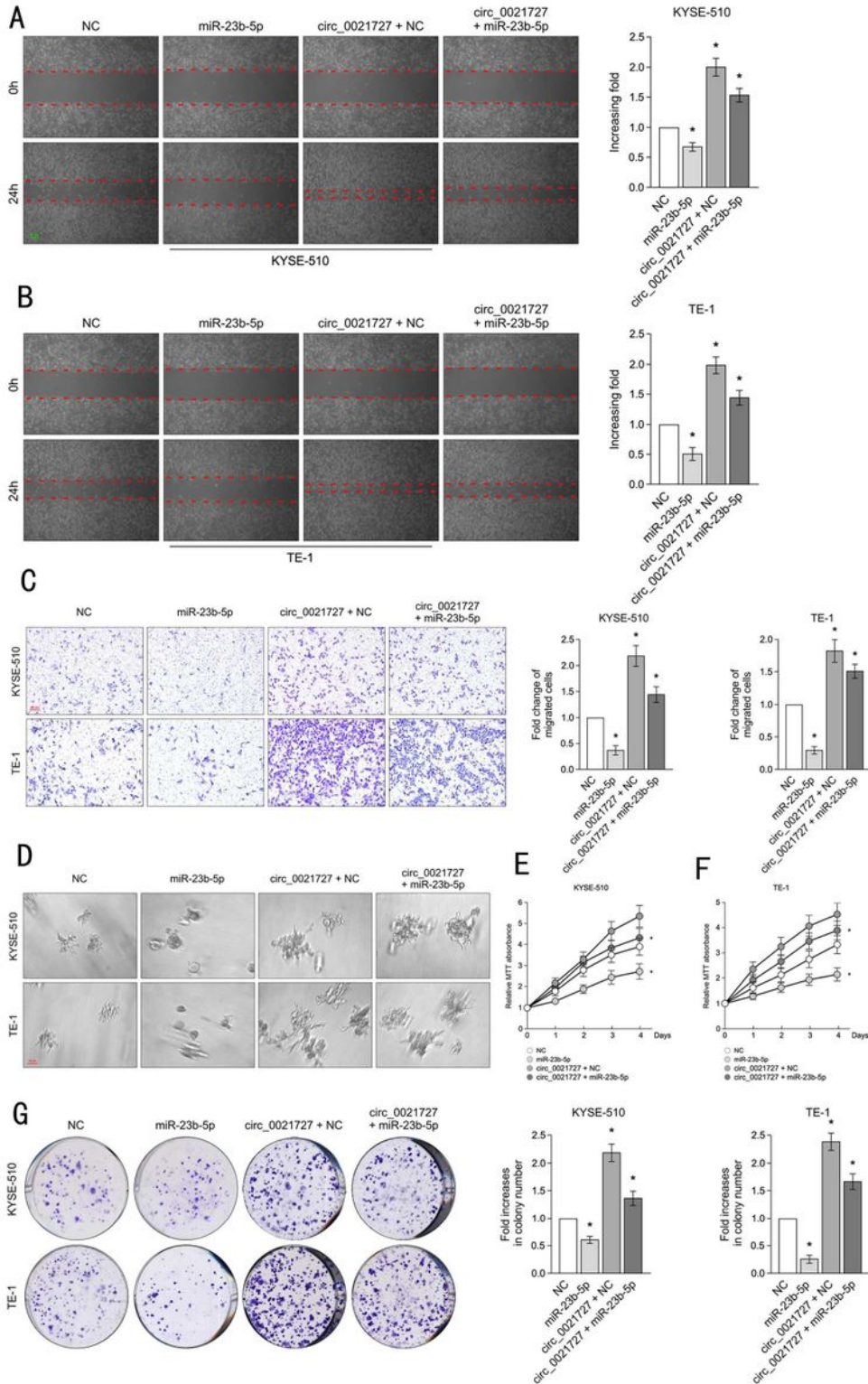


Figure 5

Hsa_circ_0021727 promotes ESCC cell proliferation, invasion and migration via miR-23b-5p. **A** and **B** The wound healing assay evaluated the cell migration ability of KYSE510 cells and TE-1 cells co-transfected with miR-23b-5p and hsa_circ_0021727 overexpression vector. **C** Transwell assays showed that miR-23b-5p and hsa_circ_0021727 jointly affected the invasion ability of KYSE510 and TE-1 cells. **D** Three-dimensional (3D) spheroid invasion assays showed the effects of hsa_circ_0021727 and miR-23b-5p on the growing antennae of KYSE510 and TE-1 cells. **E** and **F** MTT assays demonstrated the proliferation capacity of KYSE510 and TE-1 cells co-transfected with miR-23b-5p and hsa_circ_0021727 overexpression vector. **G** Colony formation assays indicated that cell proliferation capability of KYSE510 and TE-1 cells transfected with miR-23b-5p was reversed when co-transfected with hsa_circ_0021727. (Values are expressed as the means \pm SDs; *P < 0.05).

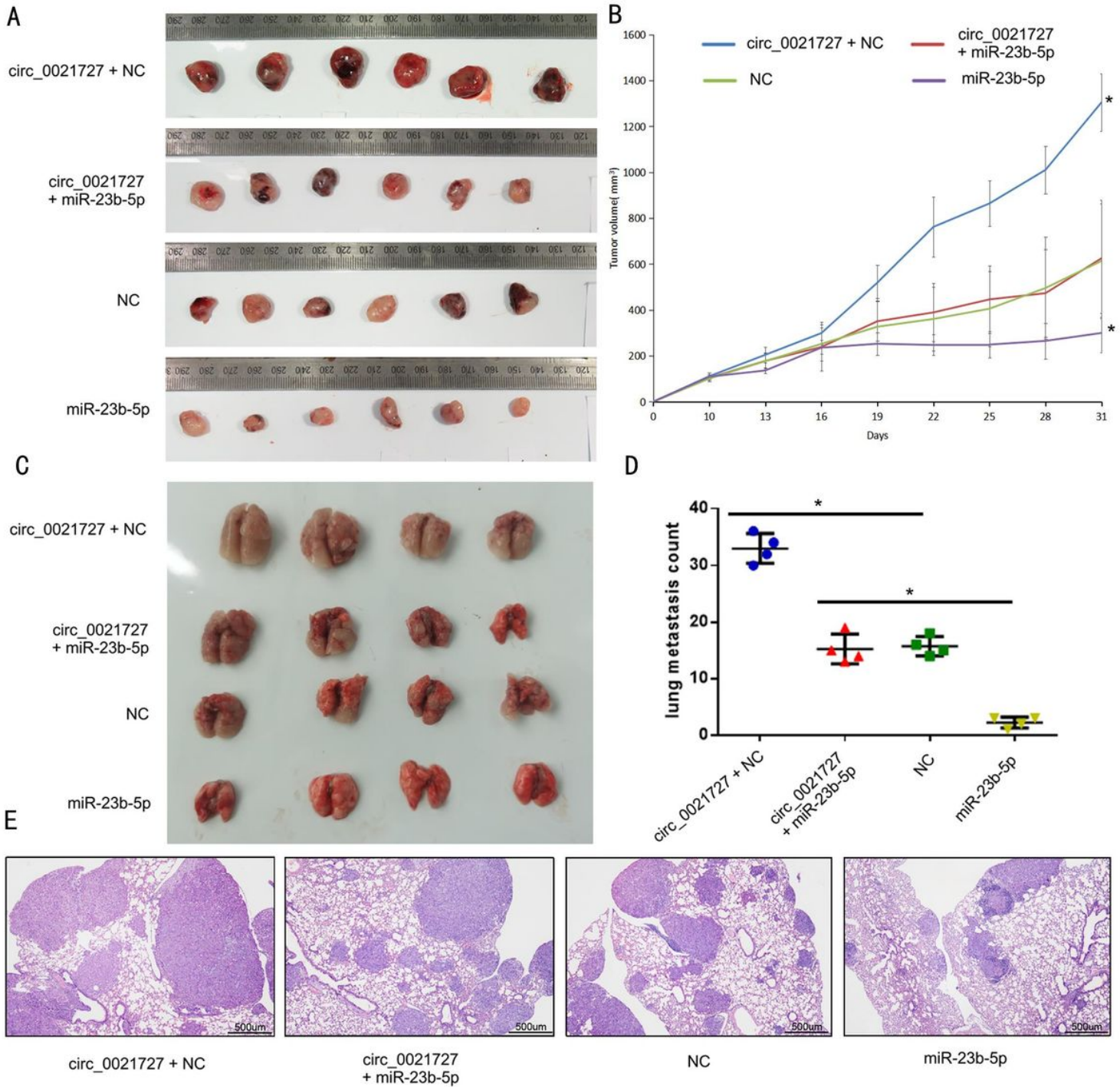


Figure 6

Hsa_circ_0021727 promotes the metastasis and proliferation of ESCC cells in vivo by regulating the expression of miR-23b-5p. **A** Image revealed subcutaneous xenograft tumor tissues injected with KYSE510 cells. KYSE510 cells co-transfected with miR-23b-5p and hsa_circ_0021727 overexpression vector. **B** Curves of tumor volumes in subcutaneous xenograft tumors models. **C** Picture of lung metastatic nodules. Nude mice were injected with KYSE510 cells co-transfected with miR-23b-5p and hsa_circ_0021727 overexpression vector. **D** Statistical analysis of lung metastatic nodules. **E** Lung tissue was stained with HE. (Values are expressed as the means \pm SDs; * $P < 0.05$).

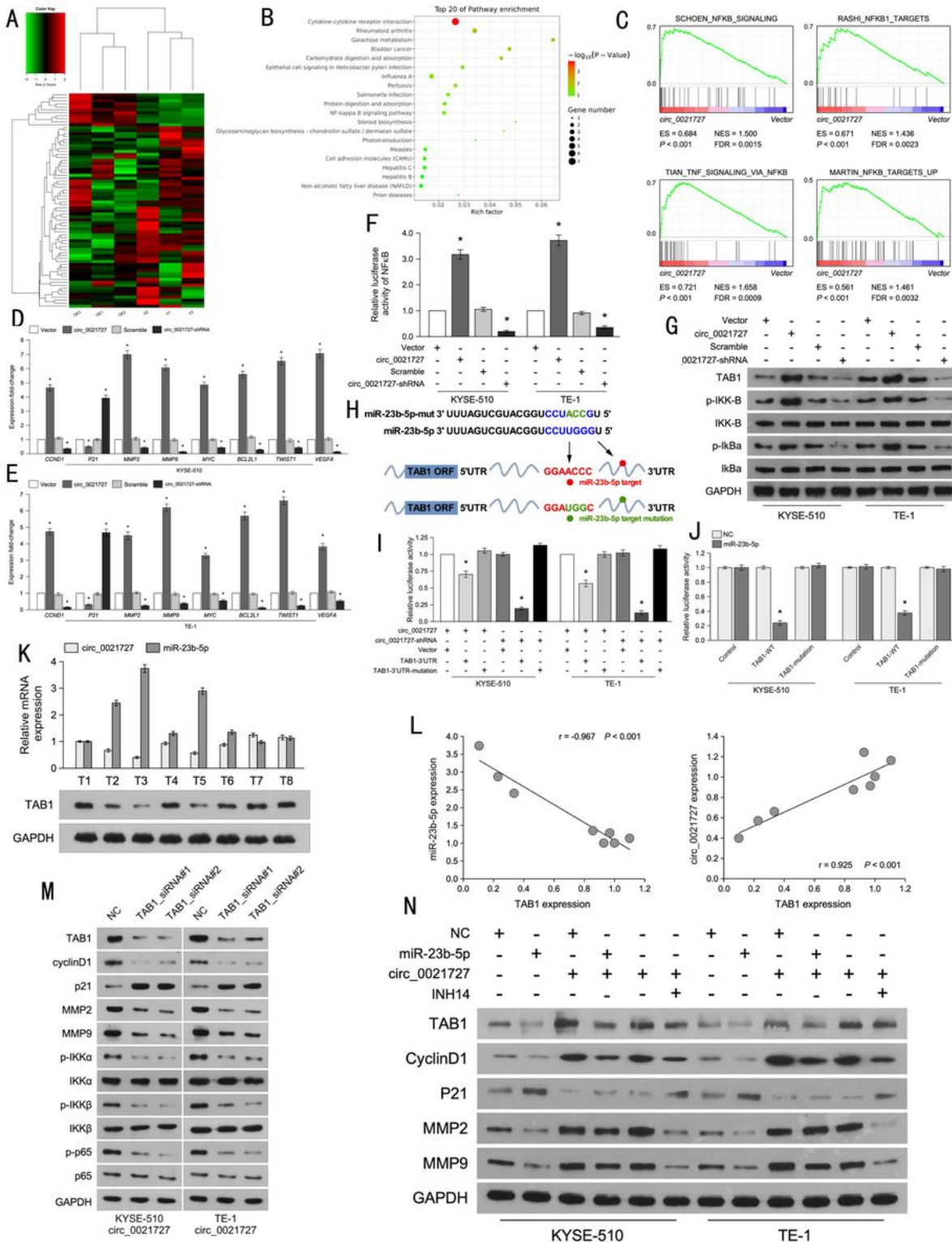


Figure 7

Hsa_circ_0021727 activates TAB1/NFκB signaling via miR-23b-5p. **A** Heatmap created from transcriptome sequencing (OE: overexpression, V: vector). **B** The top 20 pathway enrichment picture was drawn based on transcriptome sequencing results. **C** GSEA results showed that hsa_circ_0021727 was positively correlated with NFκB signaling. **D** and **E** After transfection of hsa_circ_0021727 overexpression or knockdown vector, qRT-PCR detected the expression of NFκB signaling related factors at the RNA

level.**F** After transfection of hsa_circ_0021727 overexpression or knockdown vector, the dual luciferase assay detected the luciferase activity of NFκB signaling.**G** After transfection of Hsa_circ_0021727 overexpression or knockdown vector, western blot analysis was used to detect the protein expression of TAB1 and NFκB pathway factors.**H** TAB1 mutant and wild-type sequences were designed.**I** Dual luciferase assays showed luciferase activity after co-transfection of hsa_circ_0021727 overexpression or hsa_circ_0021727-shRNA vector, TAB1 wild-type or TAB1 mutant vector.**J** Dual luciferase assays showed luciferase activity after co-transfection of miR-23b-5p overexpression vector or NC vector, TAB1 wild-type or TAB1 mutant vector.**K** qRT-PCR and western blot analysis detected the expression of hsa_circ_0021727, miR-23b-5p and TAB1 in ESCC patient tissues, respectively.**L** The correlation of hsa_circ_0021727, miR-23b-5p and TAB1 was analyzed.**M** After co-transfection of hsa_circ_0021727 overexpression vector and TAB1 knockdown vector, western blot analysis examined the protein expression of TAB1 and downstream related factors.**N** After co-transfection of hsa_circ_0021727 overexpression vector,miR-23b-5p overexpression vector, western blot analysis examined the protein expression of TAB1 and downstream related factors.After adding INH14, western blot analysis detected the protein expression of TAB1 and downstream related factors in KYSE510 cells and TE-1 cells transfected with hsa_circ_0021727 overexpression vector.(Values are expressed as the means ± SDs; *P < 0.05).

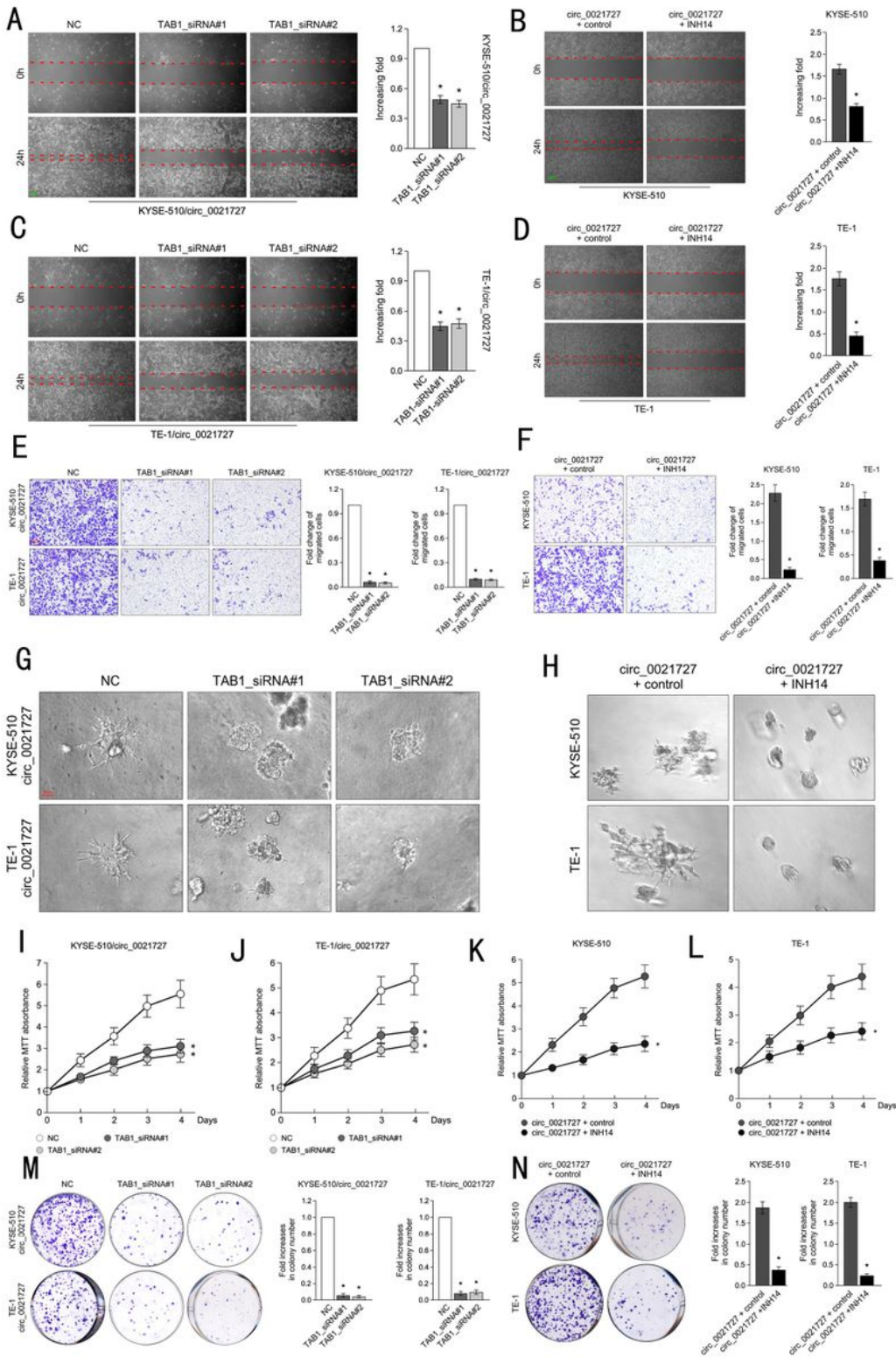


Figure 8

Hsa_circ_0021727 promotes ESCC cell proliferation, invasion and migration by activating the TAB1/NFκB pathway. **A** and **C** The wound healing assays demonstrated the migration ability of KYSE510 cells and TE-1 cells co-transfected with hsa_circ_0021727 overexpression vector and TAB1 knockdown the vector. **B** and **D** After adding INH14, the wound healing assays demonstrated the migration ability of KYSE510 cells and TE-1 cells transfected with hsa_circ_0021727 overexpression vector. **E** Transwell assays showed the

invasion ability of KYSE510 cells and TE-1 cells co-transfected with hsa_circ_0021727 overexpression vector. **F** After adding INH14, transwell assays demonstrated the invasion ability of KYSE510 cells and TE-1 cells transfected with hsa_circ_0021727 overexpression vector. **G** Three-dimensional (3D) spheroid invasion assays revealed the invasion ability of KYSE510 cells and TE-1 cells co-transfected with hsa_circ_0021727 overexpression vector, TAB1 knockdown the vector. **H** After adding INH14, three-dimensional (3D) spheroid invasion assays demonstrated the invasion ability of KYSE510 cells and TE-1 cells transfected with hsa_circ_0021727 overexpression vector. **I** and **J** MTT assays showed the proliferation ability of KYSE510 cells and TE-1 cells co-transfected with hsa_circ_0021727 overexpression vector, TAB1 knockdown the vector. **K** and **L** After adding INH14, MTT assays showed the proliferation ability of KYSE510 cells and TE-1 cells transfected with hsa_circ_0021727 overexpression vector. **M** Colony formation assays indicated that cell proliferation capability of KYSE510 and TE-1 cells co-transfected with hsa_circ_0021727 overexpression vector, TAB1 knockdown the vector. **N** After adding INH14, Colony formation assays indicated that cell proliferation capability of KYSE510 and TE-1 cells transfected with hsa_circ_0021727 overexpression vector. (Values are expressed as the means \pm SDs; * $P < 0.05$).

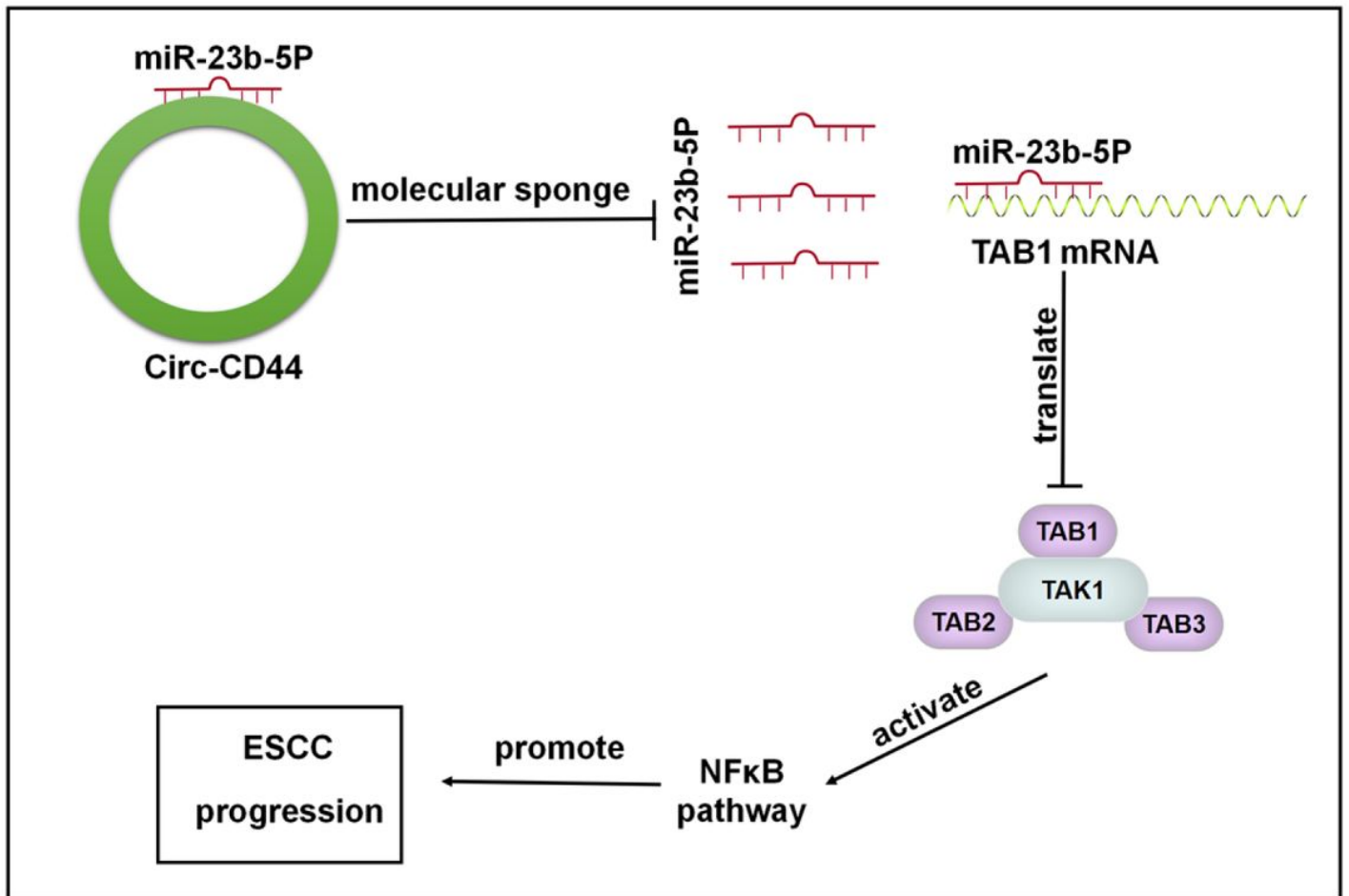


Figure 9

Legend not included with this version.

Supplementary Files

This is a list of supplementary files associated with this preprint. Click to download.

- [TableS1.doc](#)
- [TableS2.doc](#)
- [TableS3.doc](#)
- [TableS4.doc](#)